Carcinogenesis vol.34 no.6 pp.1323–1330, 2013
doi:10.1093/carcin/bgt058
Advance Access publication February 12, 2013

Inhibitory effect of oleanolic acid on hepatocellular carcinoma *via* ERK–p53-mediated cell cycle arrest and mitochondrial-dependent apoptosis

Xin Wang[†], Hua Bai[†], Xiaodi Zhang[†], Jiangzheng Liu, Peipei Cao, Nai Liao, Wei Zhang, Zhao Wang and Chunxu Hai*

Department of Toxicology, Shaanxi Key Lab of Free Radical Biology and Medicine, the Ministry of Education Key Lab of Hazard Assessment and Control in Special Operational Environment, School of Public Health, Fourth Military Medical University, Xi'an, Shaanxi 710032, China

*To whom correspondence should be addressed. Department of Toxicology, School of Public Health, Fourth Military Medical University, 169 Changle West Road, Xi'an, Shaanxi 710032, China. Tel/Fax: +86-029-84774879; Email: cx-hai@fmmu.edu.cn

Incidence of hepatocellular carcinoma (HCC) is dramatically increasing and is the third cause of cancer death worldwide. One key approach to control HCC is chemoprevention by naturally occurring agents. This study aims at investigating the antitumor effect of oleanolic acid (OA) and the molecular mechanisms. BALB/c mice were injected subcutaneously with HepG2 cells to establish transplanted tumors. Apoptosis and cell cycle arrest-related markers and signaling cascades were determined by western blot, immunofluorescence, reverse transcriptase–polymerase chain reaction and flow cytometric analysis. OA exhibited inhibitory effect on HCC through induction of apoptosis and cell cycle arrest both in transplanted tumors and in HepG2 cells. OA induced apoptosis through mitochondrial pathway, evidenced by inhibition of Akt/mammalian target of rapamycin pathway, mitochondrial dysfunction, transient increase of adenosine triphosphate, increase of Bax/Bcl-2 ratio, increased release of cytochrome c and activation of caspase/poly (ADP-ribose) polymerase. Activation of mitochondrial apoptotic pathway may be due to reactive oxygen species generated by mitochondrial fatty acid oxidation, resulted from enhancement of lipolysis regulated by cyclic adenosine 3′,5′-monophosphate response element-binding protein-hormone-sensitive lipase/peroxisome proliferator-activated receptor γ signaling. OA induced G_2/M cell cycle arrest through p21-mediated downregulation of cyclin B1/cdc2. Cyclooxygenase-2 (COX-2) and p53 were involved in OA-exerted effect, and extracellular signal–regulated kinase-p53 signaling played a central role in OA-activated cascades responsible for apoptosis and cell cycle arrest. OA demonstrated significant antitumor activities in HCC *in vivo* and *in vitro* models. These data provide new insights into the mechanisms underlying the antitumor effect of OA.

Introduction

Hepatocellular carcinoma (HCC) is the fifth most common cancer in men and the eighth most common cancer in women (1). The incidence of HCC is dramatically increasing and is the third cause of cancer death worldwide (2), which is a tumor with poor prognosis and few treatment options (3). To date, surgery remains the best choice of treatment that could prolong survival for HCC patients. However, there is only 10–15% incidence that is suitable for exairesis at diagnosis, leading to catastrophic outcomes for inoperable HCC. In addition to surgery, one key approach to control HCC is chemoprevention, in which process one or more non-toxic naturally occurring or synthetic agents were administrated and disease may be prevented, improved or reversed substantially. In this regard, naturally occurring triterpenoids are receiving more and more attention because of their promising efficacy in various cancer models.

As a natural triterpenoid, oleanolic acid (OA) is an aglycone of many saponins. OA exists extensively in food products (vegetable oils) and is a constituent of the leaves and roots of *Olea europaea*, *Viscum album* L., *Aralia chinensis* l. and other more than 120 plant species. OA exhibits various biological properties, including anti-inflammatory, antidiabetic and hepatoprotective effects. After absorption, OA is mainly distributed and transformed in the liver. It has been shown that OA protects mice from various hepatotoxicants such as carbon tetrachloride, acetaminophen, bromobenzene and thioacetamide (4–6). Indeed, OA has been used in Chinese medicine for the treatment of liver disorders for over two decades, such as viral hepatitis. In recent years, accumulating evidence has shown that OA exhibits potent antitumor activity against many tumor cell lines. However, the effects of OA on tumor growth have not been investigated in detail, and the underlying mechanisms responsible for antitumor effect of OA are still far from completely known.

The purpose of this study was to (i) determine the effect of OA on transplanted tumor growth in mice and HepG2 cell proliferation, (ii) study the effect of OA on apoptosis and cell cycle progression in tumors and cells and (iii) elucidate the molecular mechanisms of OA-induced apoptosis and cell cycle arrest.

Abbreviations: ATP, adenosine triphosphate; COX, cyclooxygenase; CREB, cyclic adenosine 3′,5′-monophosphate response element-binding protein; cyto c, cytochrome c; ERK, extracellular signal–regulated kinases; FAO, fatty acid oxidation; FFAs, free fatty acids; HCC, hepatocellular carcinoma; HOA, high dose of OA; HSL, hormone-sensitive lipase; LOA, low dose of OA; MitoQ, MitoQuinone; mRNA, messenger RNA; mTOR, mammalian target of rapamycin; OA, oleanolic acid; PARP, poly (ADP-ribose) polymerase; PBS, phosphate-buffered saline; PFT-α, pifithrin-α; PGC-1α, PPAR γ coactivator α; PI, propidium iodide; PPARγ, peroxisome proliferator-activated receptor γ; Rho123, rhodamine 123; ROS, reactive oxygen species; RT–PCR, reverse transcriptase–polymerase chain reaction.

[†]These authors are coauthors of this work.

Materials and methods

Chemicals and reagents

p53, p21, peroxisome proliferator-activated receptor γ (PPARγ), hormone-sensitive lipase (HSL), cytochrome c (cyto c), cyclic adenosine 3′,5′-monophosphate response element-binding protein (CREB)-1 and β-actin antibodies were purchased from Santa Cruz Biotechnology. Extracellular signal–regulated kinase (ERK) and P-ERK antibodies were purchased from Bioworld Technology. P-Akt, P-mammalian target of rapamycin (mTOR) and COX-2 antibodies were purchased from Epitomics. Poly (ADP-ribose) polymerase (PARP) antibody, Hoechst, rhodamine 123 (Rho123) and adenosine triphosphate (ATP) assay kit were purchased from Beyotime Institute of Biotechnology. Glycerol assay kit was obtained from Applygen Technology. Free fatty acids (FFAs) enzyme-linked immunosorbent assay kit was obtained from CUSABIO BIOTECH. CellROX Deep Red reagent, MitoSOX and BODIPY were purchased from Invitrogen. Rosiglitazone (RSG), the inhibitors and most of the chemicals and reagents used in this study were procured from Sigma.

Animal model

All animal experiments were performed according to the procedures approved by Fourth Military Medical University Animal Care and Use Committee. Approximately, 45 male BALB/c mice were purchased from the experimental animal center of Fourth Military Medical University. About 0.2 ml HepG2 cells (1×10^7/ml) of exponential growth phase were injected subcutaneously into right front axilla of mice. Ten days later, the implanted tumors were large enough to measure tumor volumes. Mice were randomly divided into three groups: control, low dose of OA (LOA) and high dose of OA (HOA). In OA-treating groups, mice were administered with 75 or 150 mg/kg/day OA (intraperitoneal), respectively, for 3 weeks. In control group, mice were offered with vehicle (2% Tween 80 in sterile saline, intraperitoneal). Mice were killed at the end of the treatment. Tumors tissues were fixed in 75% ethanol and filtered by 500 mesh to get the single cell suspension for flow cytometry analysis. Part of tumor tissues was also frozen in liquid nitrogen for western blot and reverse transcriptase–polymerase chain reaction (RT–PCR) analysis.

Cell culture and treatment

The human hepatoma cell line HepG2 was purchased from Shanghai Cell Biology, Chinese Academy of Sciences. The cells were cultured in RPMI 1640 supplemented with 10% fetal bovine serum (Gibco BRL, Rockville, MD). The experiments were conducted using serum-free RPMI 1640. Cells were seeded in 6-well plates or 96-well plates. After growing into confluence, cells were exposed to indicated concentrations of OA in the presence or absence of indicated inhibitors for certain hours. At the end, cells were harvested for the detection of RT–PCR, western blots and other analyses.

Flow cytometric analysis

Apoptosis in transplanted tumor was assessed by cell cycle analysis using flow cytometry. At the end of animal experiment, tumors tissues were fixed in 75% ethanol and filtered by 500 mesh to get the single cell suspension for flow cytometry analysis of apoptosis. Cells were harvested and re-suspended in a hypotonic fluorescent solution (50 mg/ml propidium iodide [PI] and 0.1% Triton X-100 in 0.1% sodium citrate buffer) for 1 h, at 4°C in the dark. The cell cycle was analyzed by flow cytometry (FL-2) to determine the sub-G_0/G_1 DNA content and cell cycle distribution. Subdiploid populations were considered to be apoptotic. Cellquest software was used to conduct data acquisition and analysis. The results were expressed as percentage of the DNA that was fragmented.

For the detection of apoptosis of cultured cells, annexin V/PI staining (Roche) was conducted. About 20 μl of fluorescein isothiocyanate (FITC)-labeled annexin V was mixed with 1 ml binding buffer. Then, 20 μl of PI solution was added into the buffer. Cells were incubated in the mixture at room temperature for 10 min. Then, the FITC/PI fluorescence was observed under confocal laser scanning microscopy (Olympus).

Analysis of cell viability

Cell viability was measured using 3-(4,5-dimethylthiazole-2-yl)-2,5-diphenyl tetrazolium bromide assay. Briefly, cells were seeded in 96-well plates. After growing into 50~60% confluence, cells were exposed to various concentrations of OA for certain hours, then the supernatant was discarded and cells were rinsed with phosphate-buffered saline (PBS). Then, the cells were treated with 0.5 mg/ml 3-(4,5-dimethylthiazole-2-yl)-2,5-diphenyl tetrazolium bromide (dissolved in PBS and filtered through a 0.2 mm membrane) at 37°C. Four hours later, the formazan crystals were dissolved in dimethyl sulfoxide, and the absorption values were determined at 492 nm on an automated Bio-Rad 550 microtiter plate reader.

RT–PCR

Briefly, liver and cell messenger RNA (mRNA) were isolated using trizol reagent (Invitrogen). For RT–PCR, primers for indicated genes and β-actin were designed with the aid of Clone Manager software. The RT–PCR reaction used a template complementary DNA followed by PCR amplification with *Taq* DNA polymerase in the same tube. And then, PCR products were analyzed by 1.5% agarose gel electrophoresis, stained with ethidium bromide and then photographed under ultraviolet light. The quantity of each transcript was calculated according to the instrument manual and normalized to the amount of β-actin. The sequences of each primer used in this study were shown in Supplementary Table 1, available at *Carcinogenesis* Online.

Western blot

Briefly, protein extractions were separated by using sodium dodecyl sulfate–polyacrylamide gel electrophoresis on 10% polyacrylamide gels and transferred to nitrocellulose membranes (Millipore, Billerica, MA). After blocking for 1 h with 8% skimmed milk in Tris-buffered saline (10 mM Tris, 150 mM NaCl), the membrane was incubated with indicated primary antibodies overnight at 4°C. After the membrane was washed four times for 15 min each with Tris-buffered saline and Tween-20 buffer (10 mM Tris, 150 mM NaCl and 0.1% Tween-20), it was incubated in the appropriate horseradish peroxidase-conjugated secondary antibody (diluted 1:5000 in Tris-buffered saline and Tween-20) at 37°C for 30 min. The protein bands were visualized using chemiluminescent reagents according to the manufacturer's instructions and quantified using an image analyzer Quantity One System (Bio-Rad, Richmond, CA). The protein quantifications were adjusted for the corresponding β-actin or tubulin α level.

Immunofluorescence

For immunofluorescence histochemistry, cells were fixed in a freshly prepared solution of 4% paraformaldehyde, rinsed and permeabilized with 0.1% Triton X-100 in PBS. Non-specific binding was blocked and cells were incubated overnight at 4°C with specific antibodies and then incubated with FITC or Cy3-conjugated antibodies. Hoechst was used to label nuclear DNA. Specimens were examined with a confocal microscopy (Olympus).

Determination of caspase activity

The activities of caspase-9 and -3 were assessed using commercial assay kits (Beyotime Institute of Biotechnology) according to the manufacturer's instructions.

Determination of mitochondrial superoxide anion

HepG2 cells were incubated with 40 μM OA for 16 h in the presence or absence of MitoQuinone (MitoQ; 10 μM) and rotenone (10 μM). At the end, cells were incubated with Hoechst and MitoSOX (500 nM) for 30 min at 37°C and then observed under a confocal microscopy (Olympus).

Determination of reactive oxygen species

HepG2 cells were incubated with 40 μM OA for 16 h in the presence or absence of MitoQ (10 μM) and rotenone (10 μM). At the end, cells were incubated with CellROX Deep Red reagent (a probe for reactive oxygen species [ROS], 5 μM) for 30 min at 37°C and then observed under a confocal microscopy (Olympus).

Mitochondrial membrane potential

Mitochondrial membrane potential was assessed by the retention of Rho123, a specific fluorescent cationic dye that is readily sequestered by active mitochondria, depending on their transmembrane potential. In brief, HepG2 cells were incubated with 40 μM OA for 16 h in the presence or absence of MitoQ. At the end, cells were incubated with Hoechst and Rho123 (10 μM) for 30 min at 37°C. Then, sections were examined with a laser scanning confocal microscopy (Olympus).

ATP determination

For ATP measurement, a commercially available firefly luciferase assay kit (Beyotime Institute of Biotechnology) was used. Briefly, HepG2 cells were incubated with 40 μM OA for indicated hours. After a single wash with ice-cold PBS, cells were lysed with the ATP-releasing reagent provided by the kit. Then, luciferin substrate and luciferase enzyme were added and bioluminescence was assessed by a spectroflurometer. The level of cellular ATP was converted to percentage of control.

Determination of lipolysis

Oil red O staining. HepG2 cells were treated with 40 μM OA for indicated hours, and then fixed with 4% paraformaldehyde for 15 min, rinsed with water followed by 70% ethanol and stained with oil red O solution (6 parts of saturated oil red O dye in isopropanol with 4 parts of water) for 15 min. Excess stain was removed by washing with 70% ethanol. The stained cells were finally washed with water. Then, cells were incubated with 4% Nonidet P-40 in isopropanol for 5 min to dissolve stained oil droplets. The absorbance of the dye–triglyceride complex was measured at 520 nm.

BODIPY staining. HepG2 cells were treated with 40 μM OA for 16 h and incubated with Hoechst and BODIPY (a neutral lipid probe, 3.5 ng/ml) for 30 min at 37°C and then observed under a confocal microscopy (Olympus).

Determination of products of lipolysis. HepG2 cells were treated with 40 μM OA for indicated hours. At the end, extracellular and intracellular glycerol and FFAs were detected according to the manufacturer's instructions.

Statistical analysis

All experiments were performed at least three times, and results were expressed as the means ± SD. The results were analyzed by one-way analysis of variance followed by a SNK-q test for multiple comparisons. All analyses were performed using the Statistical Package for the Social Sciences software. Data were considered statistically significant for $P < 0.05$. More specific indices of statistical significance were indicated in individual figure legends.

Results

OA inhibits tumor growth and cell proliferation and induces mitochondrial-dependent apoptosis in vivo and in vitro

The effect of OA on transplanted tumor growth in mice was examined. As shown in Table I, after the administration of OA, tumor volumes and weights were reduced significantly. The tumor inhibitory ratio in LOA and HOA groups was 31.72% and 57.24%, respectively. In HepG2 cells, low concentration of OA (20 μM) showed a protective effect on cell viability (Supplementary Figure 1A–C, available at *Carcinogenesis* Online). When the concentration of OA was higher than 40 μM, cell viability treated by OA for 4 and 24 h was evidently decreased (Supplementary Figure 1A–C, available at *Carcinogenesis* Online). About 40 μM OA decreased cell viability to 46.5% of control at 24 h (Supplementary Figure 1A–C, available at *Carcinogenesis* Online). In the following cell experiments, the

Table I. Effects of OA on the growth of transplanted tumor in mice

Group	*n*	Body weight (g)	Tumor volume (mm^3)		Tumor weight (g)	Antitumor ratio (%)
			Before OA administration	Before killing		
Control	10	30.25 ± 1.22	205.47 ± 26.32	269.36 ± 52.65	1.45 ± 0.039	—
LOA	10	27.62 ± 3.05	208.49 ± 38.19	187.46 ± 43.78*	0.99 ± 0.058*	31.72
HOA	10	23.48 ± 1.59*	206.16 ± 25.79	115.31 ± 22.61*	0.62 ± 0.064*	57.24

*$P < 0.05$, compared with control.

concentration of 40 μM OA was chosen. Supplementary Figure 1D, available at *Carcinogenesis* Online, showed that OA-treated cells shrinked and departed from the plates as the incubation prolonged. It is interesting to note that under the concentration used to induce apoptosis in HepG2 cells, OA did not affect the cell viability of QZG cells, a human normal hepatocyte cell line (Supplementary Figure 2, available at *Carcinogenesis* Online). The results indicated that the toxic effect of OA was cell-type specific.

Programmed cell death (apoptosis) is a key mechanism by which antitumor drugs kill tumor cells. Next, we detected the effect of OA on apoptosis in tumors and HepG2 cells. As shown in Figure 1A, apoptosis in transplanted tumor was assessed by cell cycle analysis of sub-G_0/G_1 DNA content. The administration of OA significantly increased the percentage of sub-G_0/G_1 cells. In HOA group, the percentage of apoptotic cells increased to over 20% of total cell population (Figure 1A). In HepG2 cells, OA also induced remarkable apoptosis. Cells treated by OA for 16 h were mainly at early phase of apoptosis, evidenced by high staining of annexin V and low staining of PI (Figure 1B). Twenty-four hours after the treatment of OA, cells were at end phase of apoptosis, reflected by high staining of both annexin V and PI (Figure 1B).

Mitochondria plays a crucial role in the complex process of apoptosis by releasing several important pro-apoptotic molecules into the cytoplasm (7). Next, we detected the effect of OA on mitochondrial apoptotic pathway. In Supplementary Figure 3A, available at *Carcinogenesis* Online, we showed that OA decreased Rho123 fluorescence, confirming the collapse of mitochondrial membrane potential and the occurrence of mitochondrial dysfunction. The expression of Bcl-2 family, such as Bax and Bcl-2, was examined by RT–PCR. In tumors, Bax mRNA expression was upregulated by OA (Figure 1C). In HepG2 cells, OA also induced the mRNA expression of Bax after 8 and 16 h incubation (Figure 1C). In both tumors and cells, the Bcl-2 mRNA expression was inhibited by OA (Figure 1C). Figure 1D showed that the administration of OA increased cytosolic cyto c expression. OA also increased cyto c expression and release in HepG2 cells, reflected by enhanced fluorescence intensity (Figure 1E). In tumors, OA administration significantly increased caspase-9 and -3 activities (Figure 1G and I). In HepG2 cells treated by OA for 8 and 16 h, caspase-9 and -3 activities were also upregulated (Figure 1H and J). Moreover, proteolytic cleavage of PARP in tumors and HepG2 cells was determined by western blot. As shown in Figure 1K and L, OA increased the expression of cleaved PARP both in tumors and cells. Apoptosis is a distinct form of cell death, which requires energy. Zamaraeva *et al*. (8) showed that in response to apoptotic stimuli, the high level of cytosolic ATP was accompanied by activation of caspase-3 and internucleosomal DNA fragmentation. ATP level is a requisite to the apoptotic cell death process (8) and determines cell death fate by apoptosis or necrosis (9). Especially for mitochondrial apoptotic pathways, intracellular ATP is required (10). In this study, we showed that, 8 and 16 h after the incubation of cells with OA, ATP content was significantly increased (Supplementary Figure 3B, available at *Carcinogenesis* Online). In addition, Akt/mTOR pathway was examined. OA inhibited the phosphorylation of both Akt and mTOR in tumors (Figure 1M) and HepG2 cells (Figure 1N). These results demonstrated that OA inhibited tumor and cell growth and induced apoptosis through mitochondrial pathway *in vivo* and *in vitro*.

OA activates p53 and promotes mitochondrial fatty acid oxidation-induced ROS generation

ROS generation is a main cause of mitochondrial apoptosis. In order to detect whether ROS generation played a role in OA-activated mitochondrial apoptotic pathway, we measured intracellular and mitochondrial ROS using specific oxidation-sensitive probes. As shown in Supplementary Figure 4, available at *Carcinogenesis* Online, ROS in cells treated by OA for 16 h was increased, evidenced by higher fluorescence. More specifically, MitoSOX, a specific probe for mitochondrial superoxide anion, was used to detect mitochondrial ROS generation. In Figure 2A, we showed that OA treatment significantly increased MitoSOX staining.

Our previous studies found that OA regulated lipid metabolism and promoted lipolysis. In order to determine the role of lipid metabolism in OA-induced apoptosis, we examined lipolysis in OA-treated cells. As shown in Figure 2B, oil red O staining of HepG2 cells treated by OA were decreased in a time-dependent manner. In addition, OA decreased fluorescence intensity of BODIPY, a neutral lipid probe, further confirming the lipolysis-inducing effect of OA (Figure 2C). Moreover, we detected the content of products of lipolysis. As shown in Figure 2D, E and G, intracellular glycerol and FFAs and extracellular glycerol content were increased by OA. However, FFAs in medium was decreased after OA treatment (Figure 2F), indicating that FFAs preferentially participated in oxidation metabolism in cells, leading to the reduction of release to medium.

Under most conditions, elevation of FFAs contributes to ROS generation through mitochondrial fatty acid β-oxidation (FAO). In this study, we further investigated the role of FFAs in mitochondrial ROS generation and dysfunction. Carnitine palmitoyltransferase I catalyzes the transfer of FFAs from CoA to carnitine, allowing the initial transport of FFAs into mitochondria for β-oxidation. Overexpression of PPAR γ coactivator 1 α (PGC-1α) increases fatty acid oxidative capacity through regulating genes responsible for modulating lipid metabolism (11). As shown in Figure 2H and I, in tumors and cells treated by OA for 16 h, PGC-1α and carnitine palmitoyltransferase I mRNA expressions were elevated, indicating the enhancement of FAO. As shown in Supplementary Figure 4, available at *Carcinogenesis* Online, and Figure 2A, MitoQ (a mitochondrial-targeted antioxidant) and rotenone (an inhibitor of mitochondrial complex I) significantly inhibited OA-induced intracellular and mitochondrial ROS generation. Moreover, MitoQ and rotenone inhibited OA-induced cell apoptosis (Supplementary Figure 5, available at *Carcinogenesis* Online), further confirming that ROS generated by FAO was involved in OA-activated apoptotic cell death.

Then, we explored the mechanism of OA-induced lipolysis. HSL is one of the key enzymes responsible for lipolysis through hydrolyzing intracellular triacylglycerol and diacylglycerol (12). As shown in Figure 2J, OA increased the expression of HSL, evidenced by increased fluorescence under confocal microscopy. CREB is involved in lipid metabolism through regulating PPAR γ. In this study, in tumors and cells treated by OA for 8 and 16 h, CREB-1 expression was increased evidently (Figure 2K and L). In addition, PPAR γ expression was inhibited by OA both in tumors and cells (Figure 2K and L). The PPAR γ agonist, RSG, was used to study the role of inhibitory effect of PPAR γ on OA-induced apoptosis. Supplementary Figure 5, available at *Carcinogenesis* Online, showed that RSG significantly inhibited OA-induced annexin V/PI staining, indicating that inhibition of

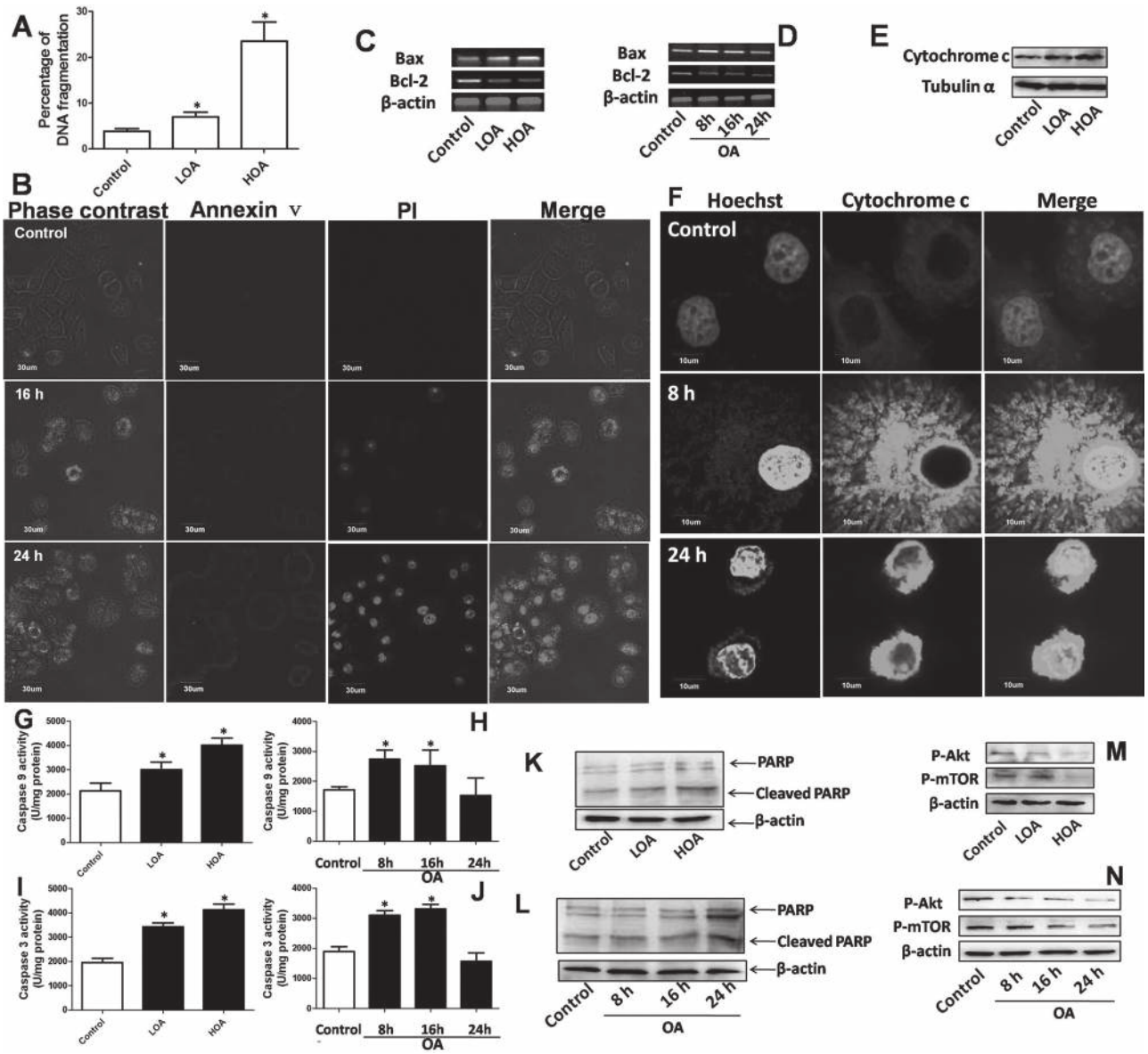

Fig. 1. The effect of OA on apoptosis in transplanted tumor in mice and HepG2 cells *in vitro*. (**A**) After transplantation of tumor cells, mice were administrated with OA for 3 weeks. At the end, tumors were collected and apoptosis was evaluated by cell cycle analysis. Percentage of sub-G_0/G_1 DNA content was shown. (**B**) HepG2 cells were treated with 40 μM OA for indicated hours. Annexin V FITC/PI double staining was conducted to observe the effect of OA on apoptosis *in vitro*. Representative images were shown. (**C** and **D**) Effect of OA on Bax and Bcl-2 mRNA expression in tumors and HepG2 cells was evaluated by RT–PCR. (**E**) Effect of OA on cyto c release in tumors was measured by western blot analysis of cytosolic protein. Representative blots were shown. (**F**) Effect of OA on cyto c release in HepG2 cells was measured by immunofluorescence using confocal microscopy. Representative images were shown. (**G**–**J**) Effect of OA on caspase 9 and -3 activities in tumors and HepG2 cells was determined by commercial kits. Results were expressed as means ± SD. (**K**–**N**) Effect of OA on proteolytic cleavage of PARP and phosphorylation of Akt and mTOR in tumors and HepG2 cells was determined by western blot. Representative blots were shown. **P* < 0.05, compared with control.

PPAR γ was involved in OA-induced apoptotic cell death. As a kind of fatty acid metabolites, COX is implicated in essential aspects of cellular signaling especially the induction of apoptosis (13). In this study, COX-2 was elevated in OA-treated tumors and in cells incubated with OA for 8 and 16 h (Figure 2K and L). NS398, an inhibitor of COX-2 activity, significantly prevented annexin V/PI staining induced by OA, confirming the involvement of COX-2 in OA-induced apoptosis (Supplementary Figure 5, available at *Carcinogenesis* Online).

The p53 tumor suppressor protein is a key player in the cellular defense against tumor growth (14). In this study, we further determined the expression of p53. As shown in Figure 2K and L, p53 protein was elevated in OA-treated tumors and in cells incubated with OA for 8 and 16 h. In addition, pifithrin-α (PFT-α), an inhibitor of p53 activity, remarkably inhibited OA-induced CREB-1 and COX-2 expression, implicating that p53 was responsible for OA-induced activation of CREB-1 and COX-2 signaling. Furthermore, PFT-α inhibited OA-induced apoptosis, evidenced by decreased fluorescence of annexin V/PI (Supplementary Figure 5, available at *Carcinogenesis* Online).

OA induces G_2/M cell cycle arrest in transplanted tumor in mice and HepG2 cell in vitro

Cell cycle arrest plays an important role in the inhibition of proliferation. Next, we investigated the effects of OA on cell cycle distribution. The proportions of cells in different phases of cell cycle in tumors and cells treated by OA for 16 and 24 h were analyzed by the incorporation of PI. The results revealed that OA induced a significant increase in the number of cells within the G_2/M phase (Figure 3A and B). mRNA expression of

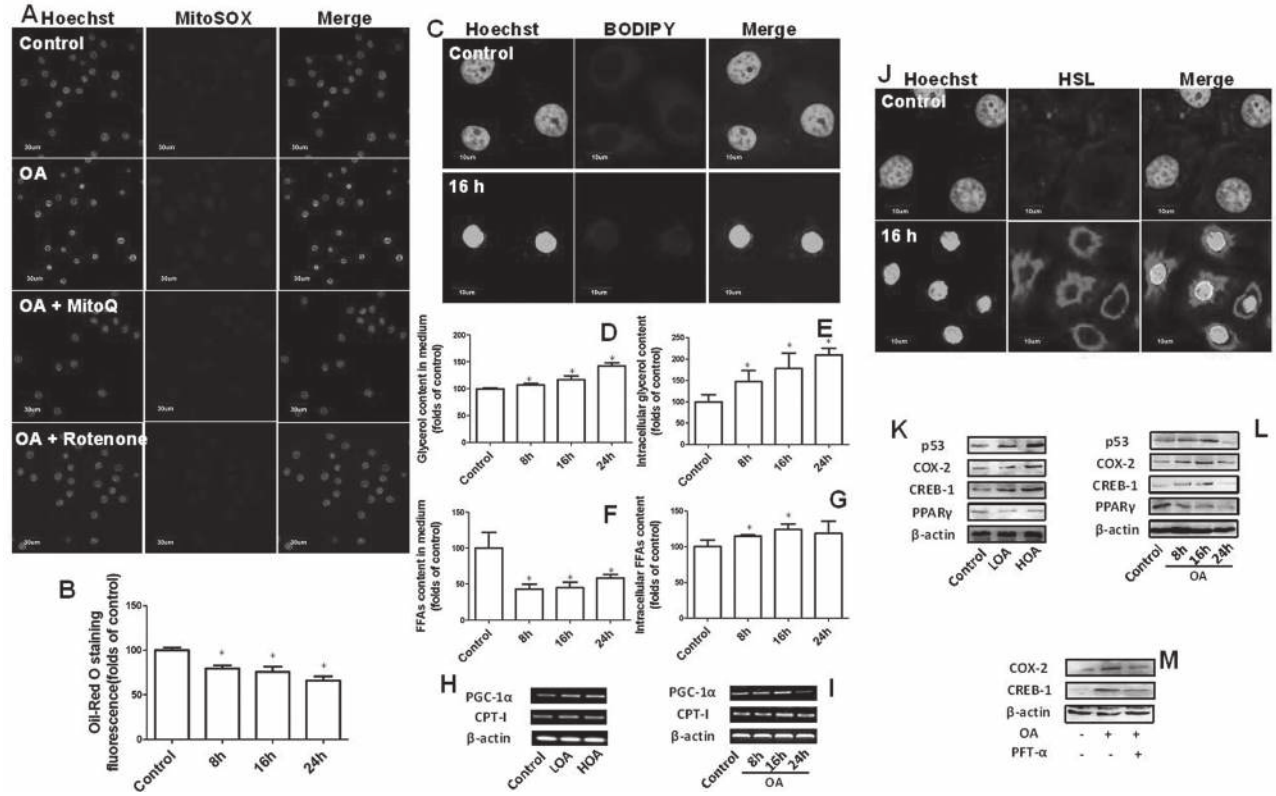

Fig. 2. The effect of OA on lipolysis and mitochondrial fatty acid oxidation in transplanted tumor in mice and HepG2 cells *in vitro*. (**A**) HepG2 cells were incubated with 40 μM OA for 16 h in the presence or absence of MitoQ (a mitochondrial-targeted antioxidant, 500 nM) and rotenone (an inhibitor of mitochondrial complex I, 10 μM). At the end, cells were incubated with Hoechst and MitoSOX (a specific probe for mitochondrial superoxide anion, 500 nM) for 30 min at 37°C and then observed under a confocal microscopy. Representative images were shown. (**B**) HepG2 cells were treated with 40 μM OA for indicated hours. Neutral lipid content was assayed by oil red O staining. Results were expressed as folds of control. (**C**) HepG2 cells were treated with 40 μM OA for 16 h and incubated with Hoechst and BODIPY (a neutral lipid probe, 3.5 ng/ml) for 30 min at 37°C and then observed under a confocal microscopy. Representative images were shown. (**D**–**G**) HepG2 cells were treated with 40 μM OA for indicated hours. At the end, extracellular and intracellular glycerol and FFAs were detected, respectively. Results were expressed as folds of control. (**H** and **I**) Effect of OA on PGC-1α and carnitine palmitoyltransferase I mRNA expression in tumors and HepG2 cells was evaluated by RT–PCR. (**J**) HepG2 cells were treated with 40 μM OA for 16 h and HSL expression was evaluated by immunofluorescence. (**K** and **L**) Effect of OA on protein expression of p53, COX-2, CREB-1 and PPARγ in tumors and HepG2 cells was determined by western blot. (**M**) HepG2 cells were treated with 40 μM OA for 16 h in the presence or absence of PFT-α, an inhibitor of p53, and then protein expression of COX-2 and CREB-1 was measured by western blot. Representative blots were shown. $^*P < 0.05$, compared with control.

cdc2 and cyclin B1, two important G_2/M phase transition checkpoints, was decreased by OA both in mice and in cells (Figure 3C and D). Moreover, in tumors and cells treated by OA for 8 and 16 h, the expression of p21 was elevated (Figure 3E and F), which was known to control the entry of cells at the G_2/M phase transition checkpoint. In the presence of PFT-α, the upregulation of p21 induced by OA was significantly inhibited (Figure 3G). Furthermore, PFT-α inhibited OA-induced G_2/M cell cycle arrest, evidenced by decrease of G_2/M phase cell population (Supplementary Figure 6, available at *Carcinogenesis* Online), indicating an important role of p53 in OA-induced cell cycle arrest *via* activating p21. In addition, as NS398 inhibited G_2/M cell population induced by OA (Supplementary Figure 6, available at *Carcinogenesis* Online), COX-2 was also involved in OA-induced cell cycle arrest.

ERK–p53 signaling is responsible for OA-induced apoptosis and cell cycle arrest

Accumulating evidences indicate that activation of mitogen-activated protein kinases is associated with cell cycle arrest and apoptosis induction. Our previous studies have shown that ERK phosphorylation was involved in several effects of OA. In this study, in tumors, ERK phosphorylation was increased by OA (Figure 4A). In HepG2 cells, OA also induced a transient increase of ERK phosphorylation (Figure 4B). U0126, an inhibitor of MEK/ERK signaling, significantly inhibited OA-induced p53 expression in HepG2 cells (Figure 4C). Moreover, U0126 also inhibited apoptosis (Supplementary Figure 5, available at *Carcinogenesis* Online) and cell cycle arrest (Supplementary Figure 6, available at *Carcinogenesis* Online) induced by OA, indicating a key role of ERK in the initiation of cascades responsible for OA-exerted inhibitory effect on tumor growth and cell proliferation.

Discussion

Accumulating evidence shows that OA (15–17) and its derivatives (18–20) exhibit inhibitory effect on tumor growth *in vivo* and induce apoptosis in various tumor cells. However, the mechanism of antitumor effect of OA is still largely unknown. In this study, we investigated the inhibitory effect of OA on transplanted tumor in mice and HepG2 cell proliferation and elucidated the possible mechanisms.

The results showed that OA inhibited tumor growth in mice and HepG2 cell proliferation. Both in tumors and cells, OA induced apoptosis involving increase of Bax, decrease of Bcl-2, release of mitochondrial cyto c into the cytosol and subsequent activation of caspase-9 and -3, followed by cleavage of PARP, which was consistent with previous findings of antitumor effect of OA in other cells (21). In accordance with the results of OA derivatives (22), the inhibition of Akt/mTOR pathway was involved in OA-exhibited inhibitory effect on cell growth. It is established that lipolysis is associated with apoptosis (23). FAO products could induce signal transduction pathways involved in apoptosis (13) and FFAs could induce apoptosis in pancreatic β cells (24), hepatocytes (25), granulosa cells (26) and brain tumors (27). In addition, oxidation of

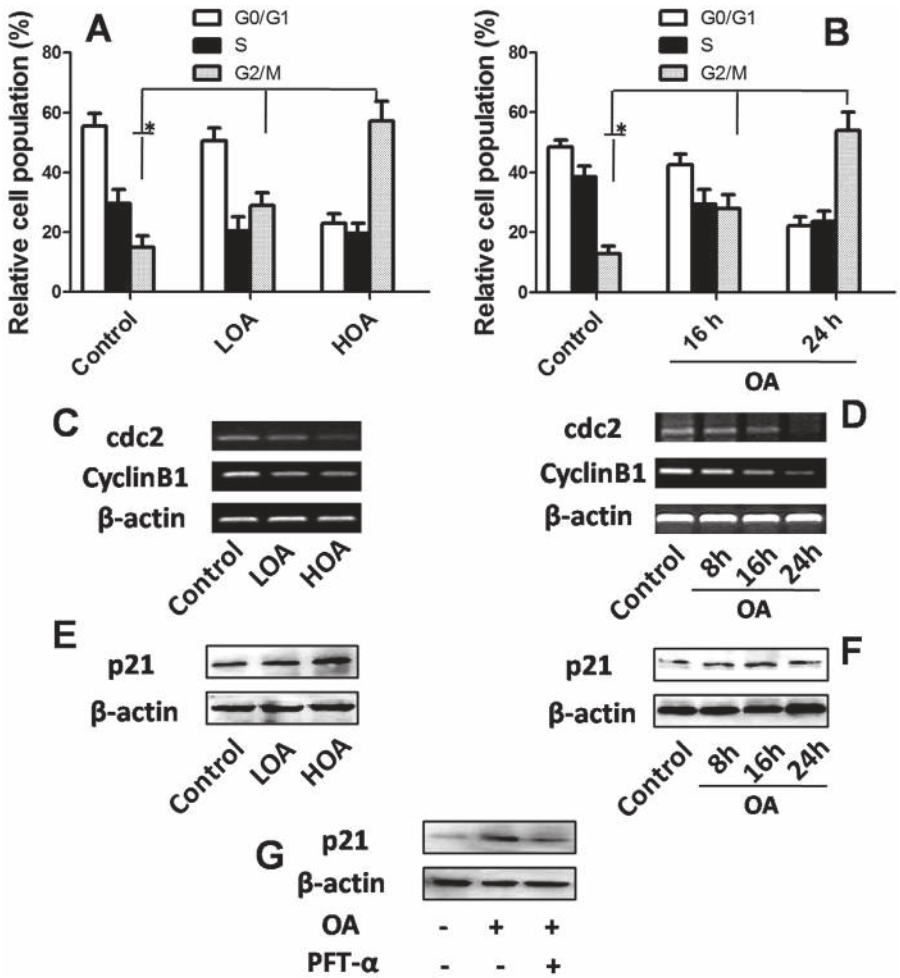

Fig. 3. The effect of OA on cell cycle progression in transplanted tumor in mice and HepG2 cells *in vitro*. (**A** and **B**) Effect of OA on cell cycle distribution in tumors and HepG2 cells was determined by flow cytometric analysis. Results were expressed as percentage of cell population. (**C** and **D**) Effect of OA on mRNA expression of cdc2 and cyclin B1 was measured by RT–PCR. (**E** and **F**) Effect of OA on protein expression of p21 was measured by western blot. (**G**) HepG2 cells were treated with 40 μM OA for 16 h in the presence or absence of PFT-α, an inhibitor of p53, and then protein expression of p21 was measured by western blot. Representative blots were shown. $^*P < 0.05$, compared with control.

FFAs is the main source of mitochondrial ROS production (28). OA was reported to arrest cell cycle and induce apoptosis *via* ROS generation in human pancreatic cancer cells (29). Gao *et al*. (30) reported that ROS was involved in CDDO-Me (an oleanane synthetic triterpenoid)-mediated growth inhibition and apoptosis in colorectal cancer cells. In this study, the activation of mitochondrial apoptotic pathway may be due to elevated ROS level, generated by FAO resulted from enhancement of lipolysis induced by OA because specific antioxidant and inhibition of mitochondrial FAO could inhibit OA-induced ROS generation and apoptosis.

In addition, upregulation of HSL, a rate-limiting enzyme of lipolysis, and downregulation of PPARγ, an important transcription factor responsible for adipogenesis and lipid accumulation, may be involved in the regulation of lipid metabolism by OA. The apoptosis-inhibitory effect of RSG further indicated the involvement of lipolysis in OA-induced apoptosis. CREB is involved in lipolysis, which is known to be stimulated by cyclic adenosine 3′,5′-monophosphate pathway (31). Mice exhibiting lower expression of CREB display higher liver triglyceride content than wild-type littermates (32). It is also reported that CREB controls hepatic lipid metabolism through PPARγ (32) and activates FAO programs by stimulating expression of PGC-1α (33). In this study, activation of CREB was induced by OA, which may be involved in the increase of HSL and the inhibition of PPARγ, leading to accumulation of lipolysis products, and activation of FAO, resulting in mitochondrial ROS generation and dysfunction.

Furthermore, we also detected the effect of OA on cell cycle distribution. Both in transplanted tumors and cells, OA induced G_2/M cell cycle arrest. G_2/M progression of cell cycle is driven by the maturation promoting factor, a complex of cyclin B1/cdc2. p21 is reported to control the entry of cells at the G_2/M phase transition checkpoint through inhibiting cyclin B1/cdc2. p21-mediated inhibition of cyclin B1/cdc2 may also play a role in OA-induced G_2/M cell cycle arrest.

COX-2, a rate-limiting enzyme in prostaglandin synthesis, is paradoxically related to cancer cell growth. A number of evidence demonstrates that COX-2 and its product PGE_2 are actors of cancer promotion and progression (34). However, recent evidence also suggests that COX-2 may be pro-apoptotic and is involved in the apoptotic effect of apoptosis inducers (35,36). Intracellular PGE2 induced an apoptotic cell death, which was dependent on the expression of the pro-apoptotic protein Bax (37). Moreover, overexpression of COX-2 could induce cell cycle arrest (38). Our results demonstrate that COX-2 activation is involved in OA-induced apoptosis and cell cycle arrest because inhibition of COX-2 could reduce OA-exerted annexin V and PI staining and G_2/M cell accumulation.

p53 regulates cell cycle and apoptosis through transcriptional modulation of a myriad of genes, which have been shown to possess antitumorigenic functions. For example, p53 induces apoptosis through promoting the transcription of pro-apoptotic genes such as Bax, release of cyto c and the activation of pro-caspase-3 and

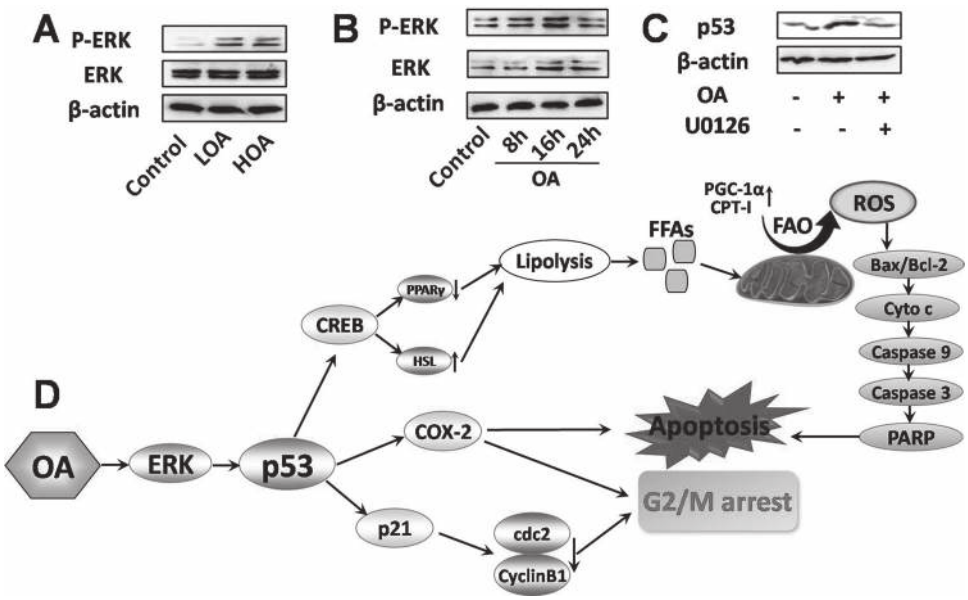

Fig. 4. The effect of OA on ERK signaling in transplanted tumor in mice and HepG2 cells *in vitro*. (**A** and **B**) Effect of OA on ERK phosphorylation was measured by western blot. Representative blots were shown. (**C**) HepG2 cells were treated with 40 μM OA for 16 h in the presence or absence of U0126, an inhibitor of MEK/ERK, and then protein expression of p53 was measured by western blot. Representative blots were shown. (**D**) Proposed schematic diagram of the events underlying the inhibitory effect of OA on HCC.

repressing the transcription of antiapoptotic Bcl-2 (39,40). p53 is also shown to induce G_2/M arrest *via* p21-mediated downregulation of cyclin B1/cdc2 (41). In this study, OA increased p53 expression and inhibition of p53 suppressed OA-induced CREB-1, COX-2 and p21 expression, indicating a pivotal role of p53 in the upstream of OA-exerted apoptotic cascades, leading to both apoptosis and cell cycle arrest. As a signaling molecule for survival and differentiation pathway, ERK has recently been identified to be involved in apoptosis (42) and PARP signaling (43). In human adipocytes, tumor necrosis factor-α stimulates lipolysis through activation of MEK/ERK and subsequent activation of cyclic adenosine 3′,5′-monophosphate signaling (44). In resveratrol-induced ovarian cancer cell apoptosis, activation of ERK is responsible for the upregulation of COX-2 (35). In this study, OA activated ERK and inhibition of ERK blocked OA-induced p53 expression and thus apoptosis and cell cycle arrest.

In conclusion, this study has found that OA exhibits inhibitory effect on HCC through inducing apoptosis and cell cycle arrest both in transplanted tumors and in HepG2 cells. OA induces mitochondrial-dependent apoptosis through FAO-mediated mitochondrial dysfunction *via* regulation of lipolysis by CREB (Figure 4D). OA induces cell cycle arrest through p21-mediated downregulation of cyclin B1/cdc2 (Figure 4D). COX-2 and p53 are involved in OA-exerted effect, and ERK–p53 signaling plays a central role in OA-activated cascades responsible for apoptosis and cell cycle arrest (Figure 4D). Taken together, these data provide new insights into the mechanisms underlying the antitumor effect of OA and the cell-type-specific toxic effect of OA gives it superiority in becoming a promising pharmacological agent for treating cancer.

Supplementary material

Supplementary Table 1 and Figures 1–6 can be found at http://carcin.oxfordjournals.org/

Funding

National Natural Science Foundation of China (No. 30872135); Program for Changjiang Scholars, Innovative Research Team in University (PCSIRT) and Natural Science Foundation of Shaanxi Province (No. S2013JC10314).

Conflict of Interest Statement: None declared.

References

1. Llovet,J.M. *et al.* (2003) Hepatocellular carcinoma. *Lancet*, **362**, 1907–1917.
2. Parkin,D.M. (2001) Global cancer statistics in the year 2000. *Lancet Oncol.*, **2**, 533–543.
3. Aleksic,K. *et al.* (2011) Evolution of genomic instability in diethylnitrosamine-induced hepatocarcinogenesis in mice. *Hepatology*, **53**, 895–904.
4. Liu,J. *et al.* (1995) Effect of oleanolic acid on hepatic toxicant-activating and detoxifying systems in mice. *J. Pharmacol. Exp. Ther.*, **275**, 768–774.
5. Liu,J. *et al.* (1994) The effect of Chinese hepatoprotective medicines on experimental liver injury in mice. *J. Ethnopharmacol.*, **42**, 183–191.
6. Liu,J. (1995) Pharmacology of oleanolic acid and ursolic acid. *J. Ethnopharmacol.*, **49**, 57–68.
7. Wang,X. (2001) The expanding role of mitochondria in apoptosis. *Genes Dev.*, **15**, 2922–2933.
8. Zamaraeva,M.V. *et al.* (2005) Cells die with increased cytosolic ATP during apoptosis: a bioluminescence study with intracellular luciferase. *Cell Death Differ.*, **12**, 1390–1397.
9. Eguchi,Y. *et al.* (1997) Intracellular ATP levels determine cell death fate by apoptosis or necrosis. *Cancer Res.*, **57**, 1835–1840.
10. Tatsumi,T. *et al.* (2003) Intracellular ATP is required for mitochondrial apoptotic pathways in isolated hypoxic rat cardiac myocytes. *Cardiovasc. Res.*, **59**, 428–440.
11. Nikolić,N. *et al.* (2012) Overexpression of PGC-1α increases fatty acid oxidative capacity of human skeletal muscle cells. *Biochem. Res. Int.*, **2012**, 714074–714085.
12. Carmen,G.Y. *et al.* (2006) Signalling mechanisms regulating lipolysis. *Cell. Signal.*, **18**, 401–408.
13. Tang,D.G. *et al.* (2002) Fatty acid oxidation and signaling in apoptosis. *Biol. Chem.*, **383**, 425–442.
14. Murphy,M.E. *et al.* (2004) p53 moves to mitochondria: a turn on the path to apoptosis. *Cell Cycle*, **3**, 836–839.
15. Hsu,H.Y. *et al.* (1997) Effects of oleanolic acid and ursolic acid on inhibiting tumor growth and enhancing the recovery of hematopoietic system postirradiation in mice. *Cancer Lett.*, **111**, 7–13.

16. Tokuda,H. *et al.* (1986) Inhibitory effects of ursolic and oleanolic acid on skin tumor promotion by 12-O-tetradecanoylphorbol-13-acetate. *Cancer Lett*., **33**, 279–285.
17. Lúcio,K.A. *et al.* (2011) Oleanolic acid initiates apoptosis in non-small cell lung cancer cell lines and reduces metastasis of a B16F10 melanoma model *in vivo*. *PLoS ONE*, **6**, e28596.
18. Ahmad,R. *et al.* (2006) Triterpenoid CDDO-Me blocks the NF-kappaB pathway by direct inhibition of IKKbeta on Cys-179. *J. Biol. Chem*., **281**, 35764–35769.
19. Huang,D. *et al.* (2006) Anti-tumor activity of a 3-oxo derivative of oleanolic acid. *Cancer Lett*., **233**, 289–296.
20. Place,A.E. *et al.* (2003) The novel synthetic triterpenoid, CDDO-imidazolide, inhibits inflammatory response and tumor growth *in vivo*. *Clin. Cancer Res*., **9**, 2798–2806.
21. Shyu,M.H. *et al.* (2010) Oleanolic acid and ursolic acid induce apoptosis in HuH7 human hepatocellular carcinoma cells through a mitochondrial-dependent pathway and downregulation of XIAP. *J. Agric. Food Chem*., **58**, 6110–6118.
22. Gao,X. *et al.* (2011) Synthetic oleanane triterpenoid, CDDO-Me, induces apoptosis in ovarian cancer cells by inhibiting prosurvival AKT/NF-κB/mTOR signaling. *Anticancer Res*., **31**, 3673–3681.
23. Dave,S. *et al.* (2012) Inhibition of adipogenesis and induction of apoptosis and lipolysis by stem bromelain in 3T3-L1 adipocytes. *PLoS ONE*, **7**, e30831.
24. Shimabukuro,M. *et al.* (1998) Fatty acid-induced beta cell apoptosis: a link between obesity and diabetes. *Proc. Natl. Acad. Sci. U.S.A*., **95**, 2498–2502.
25. Wu,D. *et al.* (2000) Ethanol and arachidonic acid produce toxicity in hepatocytes from pyrazole-treated rats with high levels of CYP2E1. *Mol. Cell. Biochem*., **204**, 157–167.
26. Mu,Y.M. *et al.* (2001) Saturated FFAs, palmitic acid and stearic acid, induce apoptosis in human granulosa cells. *Endocrinology*, **142**, 3590–3597.
27. Willoams,J.R. *et al.* (1998) Apoptosis in human primary brain tumours: actions of arachidonic acid. *Prostaglandins Leukot Essent Fatty Acids,* **58**, 193–200.
28. Rosca,M.G. *et al.* (2012) Oxidation of fatty acids is the source of increased mitochondrial reactive oxygen species production in kidney cortical tubules in early diabetes. *Diabetes*, **61**, 2074–2083.
29. Wei,J. *et al.* (2012) Oleanolic acid arrests cell cycle and induces apoptosis via ROS-mediated mitochondrial depolarization and lysosomal membrane permeabilization in human pancreatic cancer cells. *J. Appl. Toxicol.*, doi: 10.1002/jat.2725. [Epub ahead of print]
30. Gao,X. *et al.* (2011) Role of reactive oxygen species (ROS) in CDDO-Me-mediated growth inhibition and apoptosis in colorectal cancer cells. *J. Exp. Ther. Oncol*., **9**, 119–127.
31. Saito,T. *et al.* (2007) Nobiletin enhances differentiation and lipolysis of 3T3-L1 adipocytes. *Biochem. Biophys. Res. Commun*., **357**, 371–376.
32. Herzig,S. *et al.* (2003) CREB controls hepatic lipid metabolism through nuclear hormone receptor PPAR-gamma. *Nature*, **426**, 190–193.
33. Herzig,S. *et al.* (2001) CREB regulates hepatic gluconeogenesis through the coactivator PGC-1. *Nature*, **413**, 179–183.
34. Dixon,D.A. (2004) Dysregulated post-transcriptional control of COX-2 gene expression in cancer. *Curr. Pharm. Des*., **10**, 635–646.
35. Lin,C. *et al.* (2011) Inducible COX-2-dependent apoptosis in human ovarian cancer cells. *Carcinogenesis*, **32**, 19–26.
36. Subramaniya,B.R. *et al.* (2011) Apoptosis inducing effect of plumbagin on colonic cancer cells depends on expression of COX-2. *PLoS ONE*, **6**, e18695.
37. Lalier,L. *et al.* (2011) Increase in intracellular PGE2 induces apoptosis in Bax-expressing colon cancer cell. *BMC Cancer*, **11**, 153–161.
38. Trifan,O.C. *et al.* (1999) Overexpression of cyclooxygenase-2 induces cell cycle arrest. Evidence for a prostaglandin-independent mechanism. *J. Biol. Chem*., **274**, 34141–34147.
39. Yee,K.S. *et al.* (2005) Complicating the complexity of p53. *Carcinogenesis*, **26**, 1317–1322.
40. Marchenko,N.D. *et al.* (2000) Death signal-induced localization of p53 protein to mitochondria. A potential role in apoptotic signaling. *J. Biol. Chem*., **275**, 16202–16212.
41. Giono,L.E. *et al.* (2006) The p53 tumor suppressor participates in multiple cell cycle checkpoints. *J. Cell. Physiol*., **209**, 13–20.
42. Biswas,N. *et al.* (2012) ICB3E induces iNOS expression by ROS-dependent JNK and ERK activation for apoptosis of leukemic cells. *Apoptosis*, **17**, 612–626.
43. Shen,X.J. *et al.* (2012) β,β-Dimethylacrylshikonin induces mitochondria dependent apoptosis through ERK pathway in human gastric cancer SGC-7901 cells. *PLoS ONE*, **7**, e41773.
44. Zhang,H.H. *et al.* (2002) Tumor necrosis factor-alpha stimulates lipolysis in differentiated human adipocytes through activation of extracellular signal-related kinase and elevation of intracellular cAMP. *Diabetes*, **51**, 2929–2935.

Received November 1, 2012; revised January 21, 2013; accepted February 4, 2013